

How to Simulate the Whispering-Gallery-Modes of Dielectric Microresonators in FEMLAB/COMSOL

Mark Oxborrow

National Physical Laboratory, Teddington, Middlesex TW11 0LW, United Kingdom

ABSTRACT

It is explained how FEMLAB / COMSOL Multiphysics can be configured to calculate, the frequencies, electromagnetic-field patterns, mode volumes, filling factors, radiation losses ... of the whispering-gallery modes of axisymmetric microresonators. The method exploits COMSOL's ability to accept the definition of solutions to Maxwells equations in so-called 'weak form'. As no transverse approximation is imposed, it remains accurate even for so-called quasi-TM and -TE modes of low, finite azimuthal mode order, as are relevant to applications in non-linear/quantum optics. The method's utility is exemplified by simulating various microresonators in the form of dielectric toroids and disks.

Keywords: Microresonator, microcavity, whispering gallery, WGM, simulation, finite element, FEMLAB, COMSOL

1. INTRODUCTION

Beyond a few specific geometries that admit analytic solutions (either exactly or perturbatively), wholly arbitrary electromagnetic structures can be modeled through computer-aided design (CAD) tools in conjunction with programs for numerically solving Maxwell's equations. This paper concerns itself with the modeling of a particular class of electromagnetic

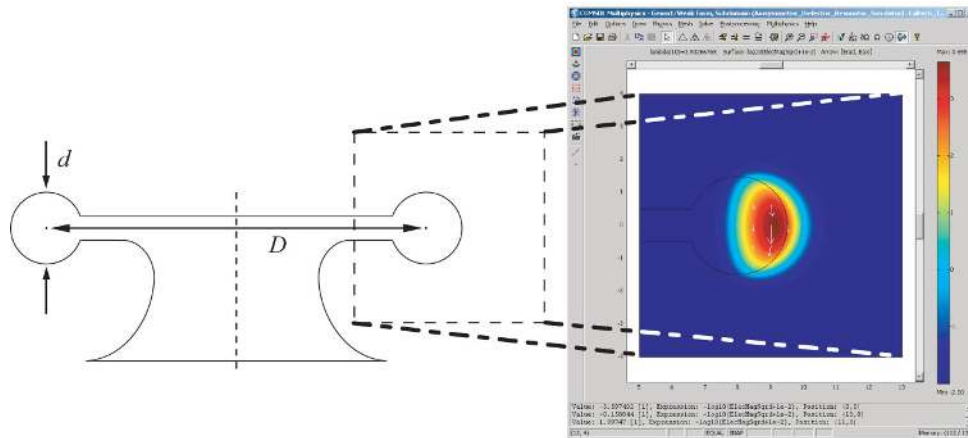


Figure 1. Leftmost: Geometry (medial cross-section) and defining dimensions of a model toroidal silica microcavity resonator –after ref. 1; the torus' principal diameter $D = 16 \mu\text{m}$ and its minor diameter $d = 3 \mu\text{m}$; the central vertical dashed line indicates the resonator's axis of continuous rotational symmetry. Rightmost: COMSOL's main panel containing a false-color ('jet') surface plot of the (logarithmic) electric-field intensity $|\mathbf{E}|^2$ for this resonator's $\text{TE}_{p=1, m=93}$ whispering-gallery mode.

structure, namely the axisymmetric resonators, that lie rather between the extremes of speciality versus arbitrariness: each such resonator exhibits a continuous rotational symmetry, but the resonator's cross-section, as viewed over a medial plane containing the rotation axis, is otherwise arbitrary (see Fig. 2). The basic modeling paradigm for this class is exemplified by Fig. 1, where, in this instance, the resonator takes the form of a toroid supported from a central mesa through an annular 'web'. Furthermore, the paper restricts itself to the simple 'circular' whispering-gallery modes (WGMs) of axisymmetric

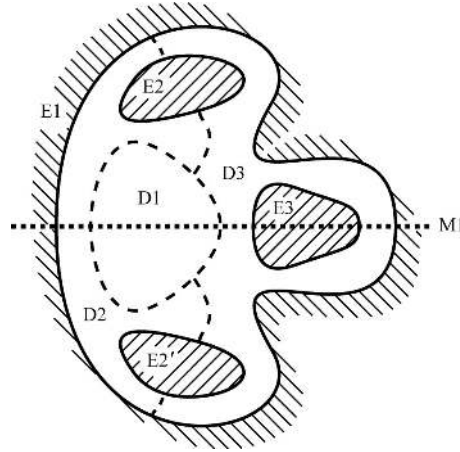


Figure 2. Generic axisymmetric resonator in cross-section (medial half-plane). A dielectric volume (in 3D) or ‘domain’ (in 2D) is enclosed by an electric wall (E1) –or one subject to some different boundary condition, as per subsection 3.5.2. This domain comprises several subdomains (D1, D2, and D3), each containing a spatially uniform dielectric (that could be just free space). Some of these subdomains (D2 and D3) are bounded internally by electric walls (E2, E2’ and E3). The resonator has (optionally) a mirror symmetry through its (horizontal) equatorial plane (dashed line M1); on imposing an electric or magnetic wall over this plane, only either the upper or lower half of the resonator need be simulated.

resonators, while acknowledging the existence of both non-planar (‘crinkled’² or ‘spooled’³) WG modes exhibiting different forms of discrete rotational symmetry, as well as those many other (non-WG) modes that exhibit either only specific reflection/inversion symmetries or no symmetries at all.

Maxwell’s equations in waveguides and resonators can be solved through the finite-element method (FEM)^{4,5} or any one of its many alternatives.^{6–13} No claims are here made as to FEM’s superior efficiency or flexibility as a modeling tool, though its convenience and accessibility are manifested by the several commercially successful software platforms^{14,15} that currently apply it. Irrespective of the method, the encoding/configurational effort required to represent Maxwell’s equations completely (such that all three field components are simultaneously solved) can be considerable, and has been absorbed within various commercial software applications or add-on modules.^{13–15} To the best of the author’s knowledge, however, no such application can be directly configured to take advantage of a circular WGM’s known azimuthal dependence, *viz.* $\exp(\pm iM\phi)$, where M (an integer ≥ 0) is the mode’s azimuthal mode order, and ϕ the azimuthal coordinate. Thus, without invasive hacking, none can implement the computationally advantageous reduction of the problem from 3D to 2D. The popular MAFIA/CST package,¹³ based on the ‘Finite Integral Method’,¹⁶ is a case in point;¹⁷ with respect to numerical efficiency, about the best one can do is simulate a ‘wedge’ [over an azimuthal domain $\Delta\phi = \pi/(2M)$ wide] between radial electric and magnetic walls.¹⁸

With circular (or, more generally, planar) whispering-gallery modes, the configurational effort can be significantly relieved by invoking a so-called ‘transverse’ approximation, whereupon only a single (scalar) partial-differential equation needs to be solved –in 2D; here, either the magnetic or electric field is assumed to lie everywhere parallel to the resonator’s axis of rotational symmetry –see figure B.1 of ref. 19. Despite this approximation’s uncontrolledness, several FEM-simulations based upon it have been reported recently.^{1,17,20} The principal purpose of this paper is to show that the transverse approximation can be avoided through only a modicum of extra effort.

If FEM is applied naively to the solving of Maxwell’s equations, spurious solutions result from the local gauge invariance, or ‘null space’²¹ of the equations’ ‘curl’ operators. These modes can be suppressed through a number of approaches: Auborg *et al*²² used a mixture of ‘Nedelec’ and ‘Lagrange’ finite elements (both 2nd order) for different components of the electric and magnetic fields; Osegueda *et al*,^{23,24} on the other hand, used a so-called ‘penalty term’ to suppress (spurious) divergence of the magnetic field. Devoid of its paraphernalia, this paper translates the latter approach into explicit, portable ‘weak-form’ expressions, suitable for direct injection into COMSOL/FEMLAB,¹⁴ thereby configuring it for the task in hand.

In the medial half plane (2D), the area covering a WG mode can be broadly divided into three regions: (i) the mode's 'near-field', covering its 'bright spot' [an annulus in full 3D] where its electromagnetic field energy is concentrated, (ii) an 'evanescent zone', lying around the near-field, where the mode's field amplitudes (and energy density) decay exponentially with distance r away from the bright spot, and (iii) a (notionally infinite) 'far field' or 'radiation zone', lying outside of the evanescent zone, where the field-amplitudes decay as $\sim 1/r$. A 'cusp' generally separates (ii) and (iii). In the case of enclosed resonators, the interior metallic (\rightarrow electric) wall of the resonator's can naturally defines the external boundary of the (necessarily finite) domain in the medial half-plane that the FEM model is defined to simulate (and 'mesh'). In the case of open resonators and their unbounded WG modes, sufficient accuracy generally requires that this boundary lie either in the radiation zone or at least deep into the evanescent zone (this point is revisited in sub-section 3.5).

2. BASIC CONFIGURATION

2.1. Weak forms

The idealized resonators considered here comprise volumes of loss-less dielectric space bounded by perfect either electric or perfect magnetic walls –as per Fig. 2. Assuming the resonator's constituent dielectric elements have negligible (or at least the same) magnetic susceptibility, the magnetic field strength \mathbf{H} will be continuous across interfaces. This property makes it advantageous to solve for \mathbf{H} (or, equivalently, the magnetic flux density $\mathbf{B} = \mu\mathbf{H}$ –with a constant global magnetic permeability μ), as opposed to the electric field strength \mathbf{E} (or displacement \mathbf{D}). It is noted here that resonators containing dielectrics with different magnetic susceptibilities could be treated at the cost of setting up 'coupling variables' (to use COMSOL's vernacular) at interfaces, but this lies beyond the scope of the present paper.

The derivation of the requisite weak forms is covered more extensively in (either of) refs. 25 and 26. Upon introducing a system of cylindrical coordinates (see top right Fig. 2), aligned with respect to the resonator's axis of rotational symmetry, and postulating time-independent solutions of the form

$$\mathbf{H}(\mathbf{r}) = e^{iM\phi} \{ H^x(x, y), i H^\phi(x, y), H^y(x, y) \}, \quad (1)$$

the resultant 'Laplacian' weak term can be shown to be

$$(\nabla \times \tilde{\mathbf{H}}^*) \cdot \frac{1}{\epsilon} (\nabla \times \mathbf{H}) = \left(\frac{A}{x} + B + xC \right) / (\epsilon_\perp \epsilon_\parallel), \quad (2)$$

where

$$A \equiv \{ \epsilon_\perp [\tilde{H}^\phi H^\phi - M(\tilde{H}^\phi H^x + H^\phi \tilde{H}^x) + M^2 \tilde{H}^x H^x] + \epsilon_\parallel M^2 \tilde{H}^y H^y \}, \quad (3)$$

$$B \equiv \epsilon_\perp [\tilde{H}_x^\phi (H^\phi - MH^x) + H_x^\phi (\tilde{H}^\phi - M\tilde{H}^x)] - \epsilon_\parallel M (\tilde{H}^y H_y^\phi + H^y \tilde{H}_y^\phi), \quad (4)$$

$$C \equiv \{ \epsilon_\perp \tilde{H}_x^\phi H_x^\phi + \epsilon_\parallel [(\tilde{H}_x^y - \tilde{H}_y^x)(H_x^y - H_y^x) + \tilde{H}_y^\phi H_y^\phi] \}. \quad (5)$$

Here, $\tilde{\mathbf{H}}$ denotes the Galerkin 'test function'⁴ of \mathbf{H} , H_x^ϕ denotes the partial derivative of H^ϕ with respect to x , *etc.*, and ϵ_\parallel and ϵ_\perp are the material's relative permittivities in the axial direction ('parallel' to the rotation axis) and 'perpendicular' plane (normal to the rot. axis), respectively. Here, the individual factors and terms have been ordered and grouped so as to display the dual symmetry between $\tilde{\mathbf{H}}$ and \mathbf{H} . Similarly, the 'penalty' weak term can be shown to be

$$\alpha (\nabla \cdot \tilde{\mathbf{H}}^*) (\nabla \cdot \mathbf{H}) = \alpha \left\{ \frac{D}{x} + E + xF \right\}, \quad (6)$$

where

$$D \equiv \tilde{H}^x H^x - M(\tilde{H}^\phi H^x + H^\phi \tilde{H}^x) + M^2 \tilde{H}^\phi H^\phi, \quad (7)$$

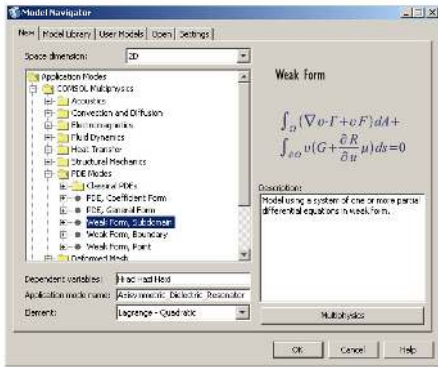
$$E \equiv (\tilde{H}_x^x + \tilde{H}_y^y)(H^x - MH^\phi) + (\tilde{H}^x - M\tilde{H}^\phi)(H_x^x + H_y^y), \quad (8)$$

$$F \equiv (\tilde{H}_x^x + \tilde{H}_y^y)(H_x^x + H_y^y). \quad (9)$$

And the temporal weak (or, in COMSOL's vernacular, the 'dweak') term is given by

$$\tilde{\mathbf{H}}^* \cdot \partial^2 \mathbf{H} / \partial^2 t = c^{-2} x (\tilde{H}^x H_{tt}^x + \tilde{H}^\phi H_{tt}^\phi + \tilde{H}^y H_{tt}^y) = -\tilde{c}^2 f^2 x (\tilde{H}^x H^x + \tilde{H}^\phi H^\phi + \tilde{H}^y H^y), \quad (10)$$

where H_{tt}^x denotes the double partial derivative of H^x with respect to time, *etc.*. Note that none of the terms on the right-hand sides of equations 2 thru 10 depend on the azimuthal coordinate ϕ ; the problem has been reduced from 3D to 2D. The Laplacian (equation 2) and dweak (equation 10) terms together encode Maxwell's equations, whereas the penalty weak term (equation 6) suppresses the spurious divergence of \mathbf{H} .



Name	Expression	Value	Description
k	2*pi/c	2.09...	
fc	k^2	4.39...	constant used internally...
alpha	10.0	10	penalty coefficient on Div H
M	11	11	azimuthal mode order
delta_e	0.0	0	fractional increment (for ...
e1	n_AlGaAs^2*(1+delta_e)	11.2...	relative permittivity of iso...
n_AlGaAs	3.36	3.36	average refractive index ...
mf	2.374616e14	2.37...	match frequency
mixing_angle	45	45	Electric-Magnetic Mixing ...
cMW	sin(mixing_angle * pi / 180)	0.70...	Magnetic-Wall-ness
cEW	cos(mixing_angle * pi / 180)	0.70...	Electric-Wall-ness
tngM	1	1	
tngE	0	0	

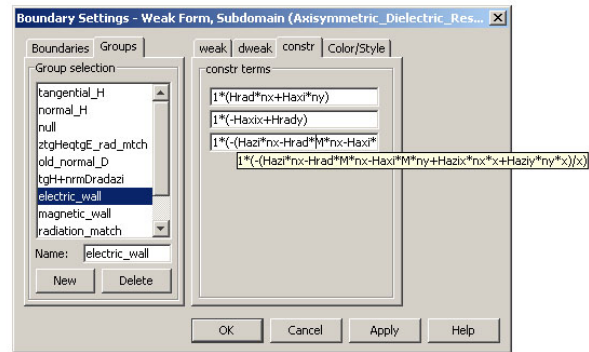
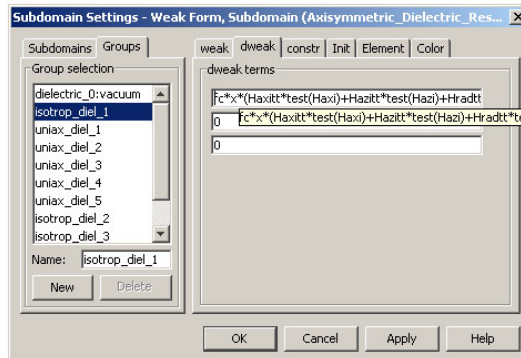
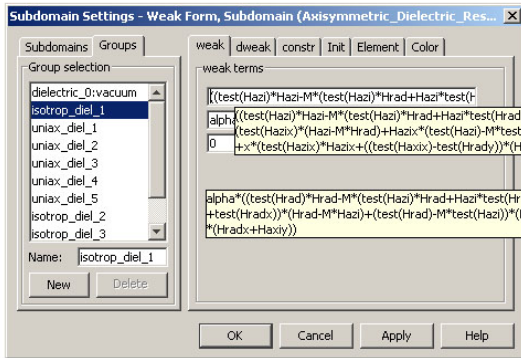


Figure 3. Configuring COMSOL in a nutshell: (a) the ‘Model Navigator’ panel indicating the selection of COMSOL’s ‘PDE Modes → Weak Form, Subdomain’ application mode (highlighted), with ‘Hrad’, ‘Hazi’, and ‘Haxi’ written in as its three (space-)‘Dependent variables’ and its ‘Element(s)’ chosen to be ‘Lagrange-Quadratic’ (actually COMSOL’s default); (b) the ‘Constants’ panel displaying the variables used in the model’s weak-form expressions and various boundary conditions (not all of these constants will in general be needed); ‘Subdomain Settings’ panel, for subdomains composed of the (isotropic dielectric) medium, ‘iso_diel_1’ (highlighted), (c) with its ‘weak’ sub-panel in view, in the upper pop-up box, the complete explicit expression for the Laplacian weak term, corresponding to equation 2, as occupies the sub-panel’s upper slot; and, in the lower pop-up box, the complete expression of the penalty weak term, corresponding to equation 6, as occupies the sub-panel’s middle slot [the remaining, lower slot of the weak sub-panel is zero-filled]; and (d) now with its ‘dweak’ sub-panel in view, in the pop-up box, the explicit expression of the temporal weak term, corresponding to equation 10, as occupies the sub-panel’s upper slot [the remaining two slots of the dweak sub-panel are zero-filled]; (e) the ‘Boundary Settings’ panel with its ‘constr(aints)’ sub-panel in view and its three slots occupied by expressions corresponding to equations 11, 12 and 14, respectively, whose values are each constrained to vanish on the boundaries to which the highlighted ‘electric wall’ boundary condition is applied; the longest such expression (as occupies the constr sub-panel’s lower slot), corresponding to equation 14, is displayed completely in a pop-up box.

2.2. Boundary conditions

An axisymmetric boundary's unit normal in cylindrical components can be expressed as $\{n_x, 0, n_y\}$ –note vanishing azimuthal component. The electric-wall boundary conditions, in cylindrical components, are as follows: $\mathbf{H} \cdot \mathbf{n} = 0$ gives

$$H^x n_x + H^y n_y = 0, \quad (11)$$

and $\mathbf{E} \times \mathbf{n} = 0$ gives both

$$H_y^x - H_x^y = 0 \quad (12)$$

and

$$\epsilon_{\perp}(H^{\phi} - H^x M + H_x^{\phi} x)n_x - \epsilon_{\parallel}(H^y M - H_y^{\phi} x)n_y = 0. \quad (13)$$

When the dielectric permittivity of the medium bounded by the electric wall is isotropic, the last condition reduces to

$$(H^{\phi} - H^x M + H_x^{\phi} x)n_x - (H^y M - H_y^{\phi} x)n_y = 0. \quad (14)$$

The magnetic-wall boundary conditions, in cylindrical components, are as follows: $\mathbf{D} \cdot \mathbf{n} = 0$ gives

$$(H^y M - H_y^{\phi} x)n_x + (H^{\phi} - H^x M + H_x^{\phi} x)n_y = 0, \quad (15)$$

and $\mathbf{H} \times \mathbf{n} = 0$ gives both

$$H^y n_x - H^x n_y = 0 \quad (16)$$

and

$$H^{\phi} = 0. \quad (17)$$

Note that the transformation $\{n_x \rightarrow -n_y, n_y \rightarrow n_x\}$, connects equations 11 and 16, and equations 14 with 15. The above weak-form expressions and boundary conditions, *viz.* equations 2 through 17 are the key results of this paper: once inserted into COMSOL, the WG modes of axisymmetric dielectric resonators can be readily calculated. Figure 3 depicts the basics of how this can be achieved within COMSOL multiphysics; the appendix of Ref. 25 provides additional instructions.

3. DERIVED QUANTITIES

Upon determining, for each mode, its frequency and all three components of its magnetic field strength \mathbf{H} as a function of position, other relevant fields and parameters can be derived from this information.

3.1. Maxwellian fields

The magnetic flux density is directly $\mathbf{B} = \mathbf{H}/\mu$. Within a dielectric, $\nabla \times \mathbf{H}(t) = \partial \mathbf{D}(t)/\partial t$, thus $\mathbf{D} = -i(2\pi f)^{-1} \nabla \times \mathbf{H}(t)$. And, $\mathbf{E} = \epsilon^{-1} \mathbf{D}$, where ϵ^{-1} is the (diagonal) inverse permittivity tensor.

Name	Expression	Description
DivH	(Hrad-Hazi*M+(Haxiy+Hradx)*x)/x	divergence of magnetic field (should ...
MagEnDens	Hrad*Hrad+Hazi*Hazi+Haxi*Haxi	magnetic energy density
Drad	(Haxi*M-Hazi*x)/x	radial component of electric displace...
Dazi	-Haxiy+Hrady	azimuthal component of electric displ...
Daxi	(Hazi-Hrad*M+Hazi*x)/x	axial component of electric displacem...
Erad	Drad/erel	radial component of electric field stre...
Eazi	Dazi/erel	azimuthal component of electric field ...
Eaxi	Daxi/erel	axial component of electric field stren...
ElecMagSqrD	Erad*Erad+Eazi*Eazi+Eaxi*Eaxi	electric field strength magnitude squ...
ElecEnDens	Erad*Drad+Eazi*Dazi+Eaxi*Daxi	electric energy density
AbsMagEnDens	abs(Hrad)^2+abs(Hazi)^2+abs(H...	
MagNrmH5qrd	2*pi*x*abs(Haxi*ny+Hrad*nx)^2	
MagTngH5qrd	2*pi*x*(1*abs(Hazi)^2+1*abs(H...	
AbsElecSqrD	abs(Erad)^2+abs(Eazi)^2+abs(E...	

Figure 4. COMSOL's Scalar Expressions Table defining how the components of the electric displacement \mathbf{D} and field strength \mathbf{E} , and other field quantities are derived from the components of the magnetic field strength \mathbf{H} .

3.2. Mode volume

With the caveats identified by Kippenberg¹⁹ in mind, the volume of a mode can be defined as²⁰

$$V_{\text{mode}} = \frac{\int \int \int_{\text{b.}-\text{s.}} \epsilon |\mathbf{E}|^2 dV}{\max[\epsilon |\mathbf{E}|^2]}, \quad (18)$$

where $\max[\dots]$, denotes the maximum value of its functional argument, and $\int \int \int_{\text{b.}-\text{s.}} \dots dV$ denotes integration over and around the mode's bright spot in the medial half-plane.

3.3. Filling factor

The resonator's electric filling factor, for a given dielectric component (labeled 'diel. '), a given mode, and a given field polarization/direction, ('dir.' \in {radial, azimuthal, axial}), is defined as

$$F_{\text{diel.}}^{\text{dir.}} = \frac{\int \int \int_{\text{diel.}} \epsilon_{\text{pol.}} |E^{\text{dir.}}|^2 dV}{\int \int \int \epsilon |\mathbf{E}|^2 dV}, \quad (19)$$

where $\int \int \int_{\text{diel.}} \dots dV$ denotes integration over the component's volume and $\text{pol.} = \{\perp, \parallel\}$ for $\text{dir.} = \{\text{radial or azimuthal, axial}\}$. The numerators/denominators of eqs. 18 and 19 can be evaluated using COMSOL's post-processing features.

3.4. Wall loss –enclosed resonators

Preamble (common to both subsection 3.4 and 3.5): The model resonator as per Fig. 2 has so-far been treated as supporting modes with infinite Q s or, equivalently, frequencies that are purely real (no imaginary part). No energy is dissipated by the dielectric material(s) within resonator (their dielectric loss tangents are presumed to be zero); none is lost through radiation –since the resonator's bounding perfect electric/magnetic walls allow none to escape; and, being perfect, the currents induced within these walls cause no resistive dissipation. Real resonators, in contrast, suffer losses that render the Q s of their modes finite. The applicability of perturbative(/inductive) methods described below requires that $Q \gg 1$.*

Now consider an enclosed resonator supporting a WG mode, where the resonator's (for simplicity single) enclosing wall is metallic and lies deep in the mode's evanescent region, and where the mode's $Q \gg 1$ is finite solely due to resistive (Ohmic) losses in this wall. To zeroth-order perturbatively, the real mode's form $\mathbf{H}(x, y)$ can be equated to that determined by solving the equivalent ideal resonator with a perfect electric as opposed to resistive wall. The energy stored in a mode's electromagnetic field is $U = (1/2) \int \int \int \mu |\mathbf{H}|^2 dV$. For axisymmetric resonators, the 3D volume integral $\int \int \int dV$ reduces to a 2D integral $\int \int (2\pi x) dx dy$ over the resonator's medial half-plane. The surface current induced in the resonator's enclosing electric wall is (see ref. 27, page 205, for example) $\mathbf{J}_s = \mathbf{n} \times \mathbf{H}$. The averaged-over-a-cycle power dissipated in the wall is $P_{\text{loss}} = (1/2) \int \int R_s |\mathbf{H}_t|^2 dS$, where \mathbf{H}_t is the tangential (with respect to the wall) component of \mathbf{H} , $R_s = (\pi f \mu / \sigma)^{1/2}$ is the wall's surface resistivity (see refs. 27, 28), σ the wall's (bulk) electrical conductivity, and f the mode's frequency. For axisymmetric resonators, the 2D surface integral $\int \int dS$ reduces to a 1D integral $\int (2\pi x) dl$ around the periphery of the resonator's medial (x-y) half-plane. The quality factor, defined as $2\pi f U / P_{\text{loss}}$, due to the wall loss can thus be expressed as

$$Q_{\text{wall}} = \frac{2\pi f \mu}{R_s} \Lambda = (4\pi f \mu \sigma)^{1/2} \Lambda, \quad (20)$$

where Λ , which has the dimensions of a length, is defined as

$$\Lambda = \frac{\int \int \int |\mathbf{H}|^2 dV}{\int \int |\mathbf{H}_t|^2 dS} = \frac{\int \int [(H^x)^2 + (H^\phi)^2 + (H^y)^2] x dx dy}{\int [|H^\phi|^2 + |H^y n_x - H^x n_y|^2] x dl}. \quad (21)$$

Again, both integrals (numerator/denominator), hence Q_{wall} , can be evaluated via COMSOL's post-processing facilities.

*Warning: As the Q of certain experimental WG-resonators can be exceedingly high ($> 10^{10}$), the amplitude of the electromagnetic field where dominant losses occur (loss rates will depend on the amplitude) can be many orders of magnitude lower than the field's maximum (or maxima) at the WG-mode's bright spot(s). The hardware and software employed to generate WG-modal solutions must thus be able to cope with such a dynamic range, lest significant numerical errors creep into the predicted (loss-rate-determining) amplitudes where the WG-resonator's supported mode is faint.

3.5. Radiation loss –open resonators

With an *open* whispering-galley-mode resonator (either microwave²⁹ or optical^{20,30}), its otherwise highly localized WG modes spread throughout free-space; energy flows away from each mode’s bright spot (where the electric- and magnetic-field amplitudes are greatest) as *radiation*.[†] Consider an enclosed equivalent of this open resonator, with an enclosing perfect electric wall now located in the WG-mode’s radiation zone. [It is noted here, for future reference, that this perfect electric wall will force the tangential component of the electric field strength to vanish everywhere on it, *i.e.* $\mathbf{E} - \mathbf{n}(\mathbf{E} \cdot \mathbf{n}) = 0$, where \mathbf{n} is the wall’s unit normal vector.] The WG mode’s form in its near-field, in the case of the ideal enclosed resonator, will be substantially the same as that in the case of the open resonator. The open WG mode’s near-field form can thus be calculated via the method developed in section 2 above, or by any other method, as applied to the enclosed resonator. Having done so, the open WG mode’s form in its radiation zone (*i.e.* its far-field ‘radiation pattern’) can be calculated by invoking the so-called *Field Equivalence Principle*,^{31,32} where the tangential components of \mathbf{E} and \mathbf{H} (or, equivalently the vector potential \mathbf{A}), calculated over any surface (in 3D) surrounding the WG mode’s bright spot, can be regarded, in Huygen’s picture, as an equivalent, secondary source of the open WG mode’s radiation. The determination of the far-field radiation pattern could thus be implemented through a standard retarded-potential (Green function) approach,^{32,33} incorporating (if necessary) a multipole expansion. And the mode’s radiation loss, hence Q , could be subsequently deduced from integrating Poynting’s vector, as derived from the radiation pattern, over all solid angles. But, such a program of work –for lack of novelty rather than utility– shall *not* be undertaken here. Instead, two different (but related) ‘trick’ methods for *estimating* the radiative Q of an open (dielectric) resonator are presented. As the first method underestimates the Q , while the second overestimates it, the two in conjunction can be used to bound the Q from below and above. Moreover, both can be implemented straightforwardly within COMSOL after the model’s geometry has been defined once and for all (*i.e.* no expansion of the model’s domain or remeshing is required). It should be added that these two methods are not restricted to axisymmetric resonators.

3.5.1. Underestimator of loss via retro-reflection

The above-considered secondary source generates an outward-going traveling wave which, but for the enclosed resonator’s wall, would lead to radiation. Instead, with the wall in place, a standing (as opposed to traveling) wave arises. Now, suppose that the shape of the (electric) wall, and its location with respect to the secondary source, is chosen to predominantly reflect the source’s outward-going wave back onto itself such that the resultant inward-going wave interferes constructively with the outgoing wave over the whole of the source’s surface. In other words (1D analogy), on regarding the enclosing wall as a short-circuit-terminated transmission line, one attempts to adjust the length of the line such that its input (analogous to the secondary source’s surface) is located at an antinode of the line’s standing wave. If such a retro-reflecting (+ phase-length adjusted) enclosing wall can be devised, then, in particular, the measured/simulated tangential magnetic field, \mathbf{H}_t , just inside of the cavity’s electric wall will be exactly *twice* that of the outward-going wave for the open resonator $\mathbf{H}_t^{\text{rad.}}$ at the same location –but without the cavity’s electric wall in place. In practice, the source will not be located exactly at an antinode (over the whole of its surface) and thus $\mathbf{H}_t > 2\mathbf{H}_t^{\text{rad.}}$. The radiation loss can be evaluated by integrating the cycle-averaged Poynting vector over the electric wall, *i.e.* $P_{\text{rad.}} = (1/2) \int \int z_0 |\mathbf{H}_t^{\text{rad.}}|^2 dS$, where z_0 is the impedance of free space. A bound on the mode’s radiative Q -factor can thus be expressed as

$$Q_{\text{rad.}} > (8\pi f/c)\Lambda, \quad (22)$$

approaching equality when the WG mode’s bright spot lies (in effect) at an antinode of the mode’s standing wave; Λ here is exactly that given by equation 21, only now the enclosing electric wall is in the radiation zone. Provided the PDE solver is able to accurately calculate the (faint) electromagnetic field on the enclosing wall in the radiation zone, it can again be readily determined. It is further remarked here that the above –admittedly rather heuristic and one-dimensional– argument, is strongly reminiscent of Schelkunoff’s induction theorem,^{31,34} which is itself a corollary of the (already-mentioned) Field Equivalence Principle. Through analogy to this theorem, the author conjectures that equation 22 holds equally well for fully vectorial waves (as governed by Maxwell’s equations) in 3D space as for scalar waves along 1D transmission lines –as argued above.

[†]As understood by Kippenberg,¹⁹ this observation implies that the support of equation 18’s $\int \int \int_{\text{b.-s.}} \dots dV$ integral (spanning the WG mode’s bright spot) must be somehow limited, spatially, or otherwise (asymptotically) rolled off, lest the integral diverge.

3.5.2. Overestimator of loss via outward-going free-space impedance matching

A complementary bound on the Q can be constructed by replacing the above enclosed resonator's electric wall with one, of the same form, that attempts to match, impedance-wise, the open resonator's radiation –and thus absorb it. For transverse, locally plane-wave radiation in the radiation zone (in free space) sufficiently far from the resonator, the required impedance-matching boundary condition on the wall is $z_0 \mathbf{n} \times \mathbf{H} = \mathbf{E} - \mathbf{n}(\mathbf{E} \cdot \mathbf{n})$, where \mathbf{n} is the wall's inward-pointing normal.[‡] Upon differentiating with respect to time and using Maxwell's displacement-current equation, this condition can, for a given mode, be generalized to

$$\cos(\theta_{\text{mix}})\{\nabla \times \mathbf{H} - \mathbf{n}[(\nabla \times \mathbf{H}) \cdot \mathbf{n}]\} + \sin(\theta_{\text{mix}})i\bar{c}f_{\text{mode}}\mathbf{n} \times \mathbf{H} = 0, \quad (23)$$

where f_{mode} is the mode's frequency, $\bar{c} \equiv 2\pi/c$ (speed of light), and θ_{mix} is a 'mixing angle'.[§] For impedance matching (with respect to an outward-going radiation), one selects $\theta_{\text{mix}} = \pi/4$, and the above equation reduces to

$$\nabla \times \mathbf{H} - \mathbf{n}[(\nabla \times \mathbf{H}) \cdot \mathbf{n}] + i\bar{c}f\mathbf{n} \times \mathbf{H} = 0. \quad (24)$$

Unless $\theta_{\text{mix}} = N\pi/2$ for integer N , the $i = \sqrt{-1}$ in equation 23 breaks the hermitian-ness of the matrix that COMSOL is required to eigensolve, leading to decaying modes with complex eigenfrequencies f_{mode} . As exploited by Srinivasan *et al.*,²⁰ the inferred quality factor for such a mode due to radiation through/into its bounding wall is given by $Q_{\text{inf.}} = \Re[f_{\text{mode}}]/2\Im[f_{\text{mode}}]$, where $\Re[\dots]$ and $\Im[\dots]$ denote taking real and imaginary parts (of the complex eigenfrequency), respectively. If the source were an infinitesimal(finite) multi-pole, then a surface in the form of a finite(infinite) sphere centered on the source, with the constraint 24 imposed on its surface, would perfectly match to the source's radiation (*i.e.* no traveling wave would get reflected back from it). In general, however, for a finite radiator, the chosen surface (necessarily of finite extent) will not lie everywhere normal to the outward-going wave's Poynting's vector and back reflections will result, leading to a smaller imaginary part in the simulated eigenmode's frequency, thus causing $Q_{\text{inf.}}$ to overestimate the true radiative Q . One may thus state

$$Q_{\text{rad.}} < \Re[f_{\text{mode}}]/2\Im[f_{\text{mode}}], \quad (25)$$

approaching equality on perfect absorption (no reflections). Again, the author conjectures that, despite the rather heuristic nature of the above argument, inequality 25 holds in general. Used together, equations 22 and 25 provide a bounded estimator on the true radiative Q .

Comment: A wholly alternative (and, one might argue, rather more 'empirical') method for estimating the radiative Q is to surround ('clad') the otherwise open resonator with sufficiently thick regions (sub-domains) of impedance-matched absorber [*i.e.*, with the absorber's dielectric constant set equal to that of free space except for a small imaginary part (loss tangent) causing the outward-going wave to be gently attenuated with little back reflection]. The 'boundary-alteration' method promoted in this paper has at least the advantage of not extending the domain of COMSOL's modeled region.

4. EXAMPLES

The codes and configuration scripts used to implement the simulations presented below are available from the author.

4.1. Toroidal silica optical resonator

The resonator modeled here¹ comprises a silica toroid, supported above a substrate by an integral interior 'web'; its geometry is shown on the left of Fig. 1. The toroid's principal and minor diameters are $\{D, d\} = \{16, 3\} \mu\text{m}$, respectively. The silica dielectric is presumed to be wholly isotropic (*i.e.*, no significant residual stress) with a relative permittivity of $\epsilon_{\text{sil.}} = 2.090$, corresponding to a refractive index of $n_{\text{sil.}} = \sqrt{\epsilon_{\text{sil.}}} = 1.4457$ at the resonator's operating wavelength (around 852 nm) and temperature. The FEM model's pseudo-random triangular mesh covered an 8-by-8 μm square [shown in dashed outlined in the centre of of Fig. 1], with an enhanced meshing density over the silica circle and its immediately

[‡]Note that the direction (polarization) of \mathbf{E} or \mathbf{H} in the wall's plane is not constrained; the two fields need only be orthogonal with their relative amplitudes in the ratio of the impedance of free space z_0 .

[§]The two terms on the left-hand side of equation 23 can be viewed as implementing electric- and magnetic-wall boundary conditions, respectively, where the (composite) boundary condition can be continuously adjusted between these two cases by varying the mixing angle θ_{mix} . [Parenthetically, $\theta_{\text{mix}} = -\pi/4$ corresponds to impedance matching *inward-coming* radiation.]

surrounding free-space; in total, the mesh comprised 5990 (base-mesh) elements, with $\text{DOF} = 36279$. Temporarily adopting Spillane *et al*'s terminology, the resonator's fundamental TE-polarized 93rd-azimuthal-mode-order mode (as shown on the right of Fig. 1, where 'TE' here implies that the polarization of the mode's electric field is predominantly aligned with the toroid's principal axis –not transverse to it) was found to have a frequency of 3.532667×10^{14} Hz, corresponding to a free-space wavelength of $\lambda = 848.629$ nm (thus close to 852 nm). Using equation 18, this mode's volume was evaluated to be $34.587 \mu\text{m}^3$; if, instead, the definition stated in equation 5 of ref. 1 is used, the volume becomes $72.288 \mu\text{m}^3$ –i.e. a factor of n_{sil}^2 greater. These two values straddle the volume of $\sim 55 \mu\text{m}^3$, for the same dimensions of silica toroid and (TE) mode-polarization, as inferred by eye from figure 4 of ref. 1.

4.2. Distributed-Bragg-reflector microwave resonator

The method's ability to simulate axisymmetric resonators of arbitrary cross-sectional complexity is demonstrated here by simulating the 10-GHz TE_{01} mode of a distributed-Bragg-reflector (DBR) resonator as analyzed by Flory and Taber (F&T)³⁵ through mode matching. One might idly speculate that analogous structures a factor of 10^4 or so smaller could be fabricated to realize high- Q optical resonators that are less limited by dielectric/surface losses.

The resonator's model geometry was generated through an auxiliary script written in MATLAB. Its corresponding mesh comprised 5476 base-mesh elements, with 66603 degrees of freedom (DOF), with 8 edge vertices for each $\sim \lambda/4$ layer of sapphire. Based on ref. 36's quartic fitting polynomials, the sapphire crystal's dielectric permittivities (at a temperature $T = 300$ K) were set to $\epsilon_{\perp} = 9.394$ (consistent with ref. 35) and $\epsilon_{\parallel} = 11.593$. The TE_{01} mode shown in Fig. 5(b) was found to lie at 10.00183 GHz, in good agreement with F&T's 'precisely 10.00 GHz'. Using equation 19, the mode's electric filling factor for the resonator's sapphire parts was 0.1270, which, assuming an (isotropic) loss tangent of 5.9×10^{-6} as per F&T, corresponds to a dielectric-loss Q factor of 1.334 million. Through equations 20 and 21, and assuming a surface resistance of 0.026Ω per square as per F&T, the wall-loss Q factor was determined to be 29.736 million, leading to a composite Q (for dielectric and wall losses operating in tandem) of 1.278 million. These three Q values are consistent with F&T's stated (composite) Q of '1.3 million, and limited entirely by dielectric losses'.

4.3. Conical microdisk optical resonator

The mode volume can be reduced by going to smaller resonators, which, unless the optical wavelength is commensurately reduced, implies *lower* azimuthal mode orders. The model 'microdisk' resonator analyzed here, as depicted in Fig. 6(a),

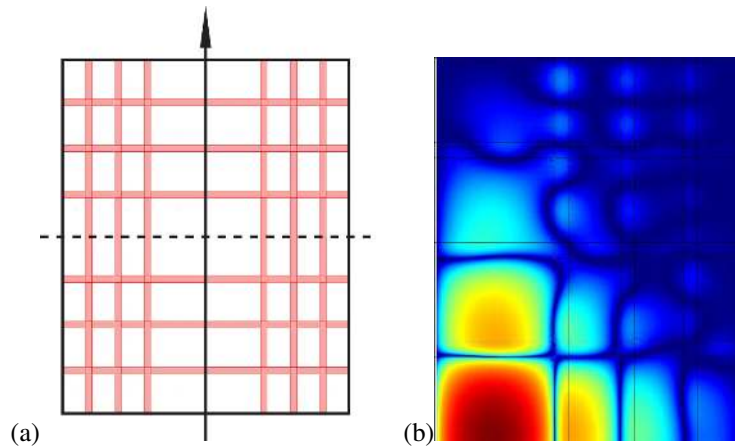


Figure 5. (a) Geometry (medial cross-section) of a 3rd-order distributed-Bragg-reflector resonator within a cylindrical metallic can (hence electric interior walls –represented by a solid black rectangle); as per ref. 35, the can's interior diameter is 10.98 cm and its interior height is 13.53 cm; the horizontal and vertical grey (or pink –in color reproduction) stripes denote cylindrical plates and barrels of sapphire; white rectangles correspond to right cylinders/annuli of free-space; the vertical arrow indicates the resonator's axis of rotational symmetry, with which the sapphire crystal's c-axis is aligned; a magnetic wall is imposed over the resonator's equatorial plane of mirror symmetry (dashed horizontal line; cf. M1 in Fig. 2). (b) False-color plot of the (logarithmic) electric-field intensity $|\mathbf{E}|^2$ over the top-right medial quadrant of the rotationally invariant ($M = 0$) TE_{01} mode; note how the mode is strongly localized within the resonator's central cylinder of free-space

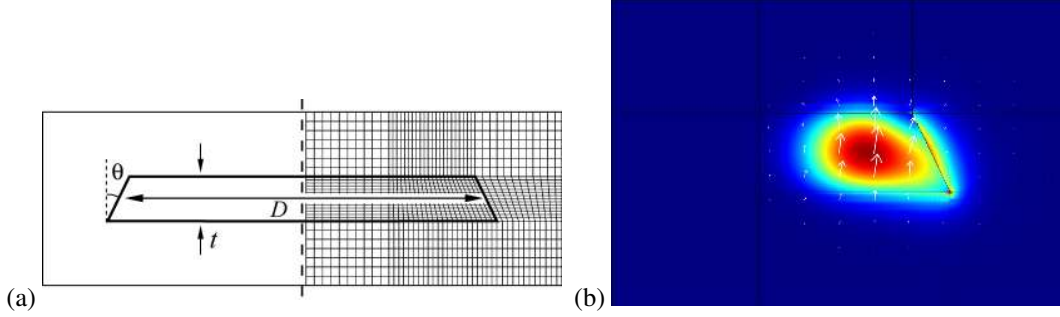


Figure 6. (a) Geometry (medial cross-section) and (half-)meshing of model GaAlAs microdisk resonator –after ref. 20; the disk’s median diameter is $D = 2.12 \mu\text{m}$ and its thickness (axial height) $t = 255 \text{ nm}$; its conical external sidewall subtends an angle $\theta = 26^\circ$ to the disk’s (vertical) axis; for clarity, only every other line of the true (full) mesh is drawn. The modeled domain in the medial half-plane is a rectangle stretching from 0.02 to $1.5 \mu\text{m}$ in the radial direction and from -0.5 to $+0.5 \mu\text{m}$ in the axial direction. (b) False-color surface plot of the (logarithmic) electric-field intensity $|E|^2$ for the resonator’s $\text{TE}_{p=1,m=11}$ mode at $\lambda = 1263.6 \text{ nm}$; again, white arrows indicate the electric field’s magnitude and direction in the medial plane.

duplicates the structure defined in figure 1(a) of Srinivasan *et al.*;²⁰ the disk’s constituent dielectric (alternate layers of GaAs and GaAlAs) is approximated as a spatially uniform, isotropic dielectric, with a refractive index equal to $n = 3.36$. The FEM-modeled domain comprised 4928 quadrilateral base-mesh elements, with $\text{DOF} = 60003$. Adopting the same authors’ notation, the resonator’s $\text{TE}_{p=1,m=11}$ whispering-gallery mode, as shown in Fig. 6(b), was found at $2.372517 \times 10^{14} \text{ Hz}$, equating to $\lambda = 1263.6 \text{ nm}$; for comparison, Srinivasan *et al* found an equivalent mode at 1265.41 nm [as depicted in their figure 1(b)]. It is pointed out here that the white electric-field arrows in Fig. 6(b) are *not* perfectly vertical –as the transverse approximation taken in references^{1,19,37} would assume them to be; the *quasi*-ness of the true mode’s transverse-electric polarization is thus revealed.

Mode volume: Using equation 18, but with the mode excited as a standing-wave (doubling the numerator while quadrupling the denominator), the mode volume is determined to be $0.1484 \times \mu\text{m}^3 \simeq 2.79(\lambda/n)^3$, still in good agreement with Srinivasan *et al*’s $\sim 2.8(\lambda/n)^3$.

Radiation loss: The $\text{TE}_{p=1,m=11}$ mode’s radiation loss was estimated by implementing both the upper- and lower-bounding estimators described in subsection 3.5. Here, the microdisk and its mode were modeled over an approximate sphere, equating to a half-disk in 2D (medial plane). The half-disk’s diameter was $12 \mu\text{m}$ and different electromagnetic conditions

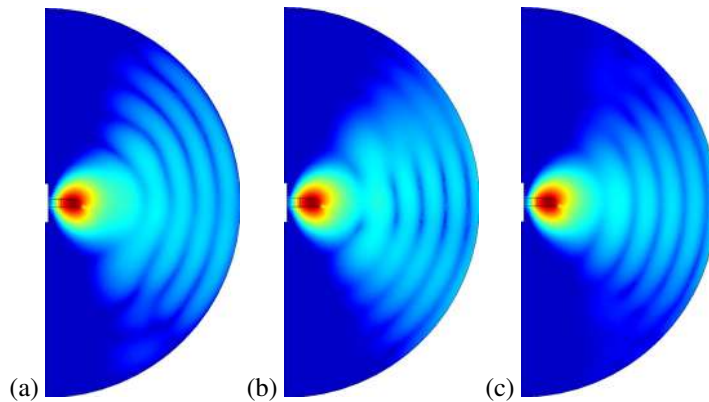


Figure 7. Radiation associated with the same [$\text{TE}_{p=1,m=11}$, $\lambda = 1263.6 \text{ nm}$] whispering-gallery mode as presented in Fig. 6 (all three maps use the same absolute false-color scale): (a) standing-wave (equal outward- and inward-going) radiation with the outer semicircular boundary set as a magnetic wall; (b) the same but now with the boundary set as an electric wall; (c) somewhat traveling (more outward- than inward-going) radiation with the boundary’s impedance set to that of an outward-going plane-wave in free space (and with the normal magnetic field constrained to vanish). That (c)’s radiation field is somewhat dimmer than (b)’s is consistent with the two different estimates of the resonator’s radiative Q corresponding to (b) and (c) [see text].

were imposed on its semicircular boundary—see Fig. 7.[¶]

With a complete electric-wall condition (*viz.* equations 11 and {12, 14}) imposed on the half-disk’s entire boundary [as per Fig. 7(b)], the right-hand of equation 22 was evaluated. And, with just the $\mathbf{E} \times \mathbf{n} = 0$ condition (equations {12, 14}) on the boundary’s semicircle replaced by the outward-going-plane-wave impedance-matching condition (*viz.* equation 23 with $\theta_{\text{mix}} = \pi/4$), while the $\mathbf{H} \cdot \mathbf{n} = 0$ condition (equation 11) is maintained, the right-hand side of equation 25 was evaluated for the radiation pattern displayed in Fig. 7(c). For a pseudo-random triangulation mesh comprising 4104 elements, with DOF = 24927, the PDE solver took, on the author’s office computer (2.4 GHz Intel Xeo CPU), 6.55 and 13.05 seconds, corresponding to Figs. 7(b) and (c), respectively,^{||} to calculate 10 eigenmodes around 2.373×10^{14} Hz, of which the $\text{TE}_{p=1,m=11}$ mode was one. Together, the resultant estimate on the $\text{TE}_{p=1,m=11}$ mode’s radiative-loss quality factor is $(1.31 < Q_{\text{rad.}} < 3.82) \times 10^7$, to be compared with the estimate of 9.8×10^6 (at 1265 nm) reported in table 1 of ref.²⁰

ACKNOWLEDGMENTS

This work was supported by the United Kingdom’s National Measurement System’s Quantum Metrology Programme.

REFERENCES

1. S. M. Spillane, T. J. Kippenberg, K. J. Vahala, K. W. Goh, E. Wilcut, and H. J. Kimble, “Ultrahigh-Q toroidal microresonators for cavity quantum electrodynamics,” *Phys. Rev. A* **71**, p. 013817, 2005.
2. M. E. Tobar, J. G. Hartnett, E. N. Ivanov, P. Blondy, and D. Cros, “Whispering gallery method of measuring complex permittivity in highly anisotropic materials: discovery of a new type of mode in anisotropic dielectric resonators,” *IEEE Trans. Instrum. and Meas.* **50**(2), pp. 522–525, 2001.
3. M. Sumetsky, “Whispering-gallery-bottle microcavities: the three-dimensional etalon,” *Opt. Lett.* **29**, pp. 8–10, 2004.
4. O. C. Zienkiewicz and R. L. Taylor, *The finite element method*, vol. 1: ‘The Basis’, Butterworth Heinemann, 5th ed., 2000.
5. B. M. A. Rahman, F. A. Fernandez, and J. B. Davies, “Review of finite element methods for microwave and optical waveguides,” *Proc. IEEE* **79**, pp. 1442–1448, 1991.
6. K. S. Kunz, *The finite difference time domain method for electromagnetics*, CRC Press, 1993.
7. N. M. Alford, J. Breeze, S. J. Penn, and M. Poole, “Layered Al_2O_3 - TiO_2 composite dielectric resonators with tuneable temperature coefficient for microwave applications,” *IEE Proc. Science, Measurement and Technology* **47**, pp. 269–273, 2000.
8. S. V. Boriskina, T. M. Benson, P. Sewell, and A. I. Nosich, “Highly efficient design of specially engineered whispering-gallery-mode laser resonators,” *Optical and Quantum Electronics* **35**, pp. 545–559, 2003. see <http://www.nottingham.ac.uk/ggiemr/Project/-boriskina2.htm>.
9. J. Ctyroky, L. Prkna, and M. Hubalek, “Rigorous vectorial modelling of microresonators,” in *Proc. 2004 6th Internat. Conf. on Transparent Optical Networks, 4-8 July 2004*, **2**, pp. 281–286, 2004.
10. J. Krupka, D. Cros, M. Aubourg, and P. Guillon, “Study of whispering gallery modes in anisotropic single-crystal dielectric resonators,” *IEEE Trans. Microwave Theory Tech.* **42**(1), pp. 56–61, 1994.
11. J. Krupka, D. Cros, A. Luiten, and M. Tobar, “Design of very high Q sapphire resonators,” *Electronics Letters* **32**(7), pp. 670–671, 1996.
12. J. A. Monsoriu, M. V. Andrés, E. Silvestre, A. Ferrando, and B. Gimeno, “Analysis of dielectric-loaded cavities using an orthonormal-basis method,” *IEEE Trans. Microwave Theory Tech.* **50**(11), pp. 2545–2552, 2002.
13. “MAFIA.” CST GmbH, Bad Nauheimer Str. 19, D-64289 Darmstadt Germany.
14. “COMSOL Multiphysics.” COMSOL, Ab., Tegnérgatan 23, SE-111 40 Stockholm, Sweden. [Online]. Available: <http://www.comsol.com/>; the work described in this paper used version 3.2(.0.224).
15. “ANSYS Multiphysics.” ANSYS, Inc., Southpointe, 275 Technology Drive, Canonsburg, PA 15317, USA.
16. D. Schmitt, B. Steffen, and T. Weiland, “2d and 3d computations of lossy eigenvalue problems,” *IEEE Trans. Magn.* **30**(5), pp. 3578–3581, 1994.

[¶]It is acknowledged that, in reality, the microdisk’s substrate would occupy a considerable part of the half-disk’s lower quadrant.

^{||}The complex arithmetic associated with the impedance-matching boundary condition caused the PDE eigen-solver to take approximately twice as long to run with this condition imposed—as compared to pure electric- or magnetic-wall boundary conditions that do not involve complex arithmetic.

17. R. Basu, T. Schnipper, and J. Mygind, "10 GHz oscillator with ultra low phase noise," in *Proc. The Jubilee 8th International Workshop 'From Andreev Reflection to the International Space Station'*, (Björkliden, Kiruna, Sweden, March 20-27, 2004), 2004.
18. M. Oxborrow, "Calculating WG modes with MAFIA." unpublished, 2001.
19. T. J. A. Kippenberg, *Nonlinear Optics in Ultra-high-Q Whispering-Gallery Optical Microcavities*. PhD thesis, Caltech, 2004. particularly Appendix B; <http://www.mpq.mpg.de/~tkippenb/TJKippenbergThesis.pdf>.
20. K. Srinivasan, M. Borselli, O. Painter, A. Stintz, and S. Krishna, "Cavity Q, mode volume, and lasing threshold in small diameter AlGaAs microdisks with embedded quantum dots," *Opt. Express* **14**, pp. 1094–1105, 2006.
21. J.-F. Lee, G. M. Wilkins, and R. Mittra, "Finite-element analysis of axisymmetric cavity resonator using a hybrid edge element technique," *IEEE Trans. Microwave Theory Tech.* **41**(11), pp. 1981–1987, 1993.
22. A. Auborg and P. Guillon, "A mixed finite element formulation for microwave device problems. application to MIS structure," *J. Electromagn. Wave Appl.* **5**, pp. 371–386, 1991.
23. R. A. Osegueda, J. H. Pierluissi, L. M. Gil, A. Revilla, G. J. Villava, G. J. Dick, D. G. Santiago, and R. T. Wang, "Azimuthally-dependent finite element solution to the cylindrical resonator," tech. rep., Univ. Texas, El Paso and JPL, Caltech, 1994. <http://trs-new.jpl.nasa.gov/dspace/bitstream/2014/32335/1/94-0066.pdf> or <http://hdl.handle.net/2014/32335>.
24. D. G. Santiago, R. T. Wang, G. J. Dick, R. A. Osegueda, J. H. Pierluissi, L. M. Gil, A. Revilla, and G. J. Villalva, "Experimental test and application of a 2-D finite element calculation for whispering gallery sapphire resonators," in *IEEE 48th International Frequency Control Symposium, 1994*, pp. 482–485, (Boston, MA, USA), 1994. <http://trs-new.jpl.nasa.gov/dspace/bitstream/2014/33066/1/94-1000.pdf> or <http://hdl.handle.net/2014/33066>.
25. M. Oxborrow, "Ex-house 2d finite-element simulation of the whispering-gallery modes of arbitrarily shaped axisymmetric electromagnetic resonators," 2006. preprint arXiv:quant-ph/0607156; contains "Configuration of COMSOL Multiphysics for simulating axisymmetric dielectric resonators: explicit weak-form expressions" as an appendix.
26. M. Oxborrow, "Traceable 2d finite-element simulation of the whispering-gallery modes of axisymmetric electromagnetic resonators," 2006. preprint arXiv:quant-ph/0611099; submitted to IEEE Transactions on Microwave Theory and Techniques.
27. U. S. Inan and A. S. Inan, *Electromagnetic Waves*, Prentice Hall, 2000. particularly subsection 5.3.2 (pp. 391-400).
28. B. I. Bleaney and B. Bleaney, *Electricity and magnetism*, Oxford University Press, 3rd ed., 1976.
29. P.-Y. Bourgeois, F. Lardet-Vieudrin, Y. Kersale, N. Bazin, M. Chaubet, and V. Giordano, "Ultra-low drift microwave cryogenic oscillator," *Electronics letters* **40**, p. 605, 2004.
30. H. Rokhsari, T. Kippenberg, T. Carmon, and K. J. Vahala, "Radiation-pressure-driven micro-mechanical oscillator," *Opt. Express* **13**, pp. 5293–5301, 2005.
31. S. A. Schelkunoff, "Some equivalence theorems of electromagnetic and their application to radiation problems," *Bell Syst. Tech. J.* **15**, pp. 92+, 1936.
32. C. A. Balanis, *Antenna Theory*, Wiley, 1997. particularly chapter 12.
33. S. Ramo, J. R. Whinnery, and T. van Duzer, *Fields and Waves in Communications Electronics*, John Wiley & Sons, 2nd ed., 1984.
34. S. A. Schelkunoff, "On diffraction and radiation of electromagnetic waves," *Physical Review* **56**(4), pp. 308 LP – 316, 1939.
35. C. A. Flory and R. C. Taber, "High performance distributed bragg reflector microwave resonator," *IEEE Trans. Ultrason. Ferroelect. Freq. Contr.* **44**(2), pp. 486–495, 1997. specifically, the mode corresponding to figures 1, 2 and 7, and the last three paragraphs of section IV, therein.
36. C. A. Flory and R. C. Taber, "Microwave oscillators incorporating cryogenic sapphire dielectric resonators," in *IEEE International Frequency Control Symposium 1993*, pp. 763–773, 1993.
37. P. Wolf, M. E. Tobar, S. Bize, A. Clairon, A. Luiten, and G. Santarelli, "Whispering gallery resonators and tests of Lorentz invariance," *General Relativity and Gravitation* **36**(10), pp. 2351 – 2372, 2004. preprint version: arXiv:gr-qc/0401017 v1.